Measurement of neutron energy spectra behind shielding at 120 GeV/c hadron beam facility, CERF

N. Nakao,[1*] **S. Taniguchi,**[2] **S.H. Rokni,**[1] **S. Roesler,**[3] **M. Brugger,**[3]
M. Hagiwara,[4] **H. Vincke,**[1,3] **H. Khater,**[1] **A.A. Prinz**[1]
[1]Stanford Linear Accelerator Centre (SLAC), USA
[2]Japan Synchrotron Radiation Research Institute (JASRI), Japan
[3]CERN, Switzerland
[4]Cyclotron Radioisotope Centre (CYRIC), Japan

Abstract

Neutron energy spectra were measured behind the lateral shield of the CERF (CERN-EU High Energy Reference Field) facility at CERN with a 120 GeV/c positive hadron beam (a mixture of mainly protons and pions) on a cylindrical copper target (7-cm diameter by 50-cm long). NE213 organic liquid scintillator (12.7-cm diameter by 12.7-cm long) was located at various longitudinal positions behind shields of 80- and 160-cm thick concrete and 40-cm thick iron. Neutron energy spectra in the energy range between 32 MeV and 380 MeV were obtained by unfolding the measured pulse height spectra with the detector response functions which have been experimentally verified in the neutron energy range up to 380 MeV in separate experiments. Since the source term and experimental geometry in this experiment are well characterised and simple, and results are given in the form of energy spectra, these experimental results are very useful as benchmark data to check the accuracies of simulation codes.

* Present address: Fermilab, MS220, P.O. Box 500, Batavia, IL 60510, USA.

1 Introduction

Estimates of high-energy neutron production and transmission through shielding are very important at high-energy electron and hadron accelerator facilities because high-energy neutrons have high penetrability through shielding and contribute significantly to external dose. Modern Monte Carlo codes provide reliable predictions of radiation fluences in accelerator facilities even for complicated facility structures. However, accuracies for the production and transmission of secondary neutrons generated by high energy beams, especially above 1 GeV, are not well known because of lack of experimental data.

This paper reports the shielding experiment at CERN carried out in August 2004. Several recent shielding experiments in accelerator facilities with high-energy neutrons are summarised in Table 1, and their characteristics are compared with those of this work. Distinctive features of this work are highest particle energy (120 GeV/c) and the variety of measured angles (13-133 degrees). Also, various thicknesses of typical shielding materials (concrete and iron) are used, and results are given as neutron-energy spectra outside the shield. The CERF facility has a simple structure of beam line and shielding, and the source term is clearly defined. The data constitute a useful benchmark to verify the accuracy of radiation transport codes.

2 CERF facility

This experiment was performed at the 120 GeV/c hadron beam line facility CERF at CERN, which was developed to provide a neutron calibration field outside the shield [10].

2.1 Shielding structure and material

This facility has a comparatively simple structure of beam line and shielding, and the source term is clearly defined. Figure1 shows the beam line of the CERF facility with 80- or 160-cm thick concrete for side shields and 80-cm thick concrete and 40-cm thick iron for roof shield. Densities of shielding materials and composition of the concrete shield are given in Tables 2 and 3, respectively. The iron roof consists of two kinds of iron materials of 20-cm thickness as shown in Figure 1.

2.2 Beam line and target

The beam line is inclined horizontally at approximately 2.1 degrees as shown in Figure 1. A copper target (50-cm thick, 7-cm diameter) was placed at two different locations, A or B, as shown in Figure 1. An activation experiment was performed simultaneously: small irradiation samples were placed behind the target and water bottles were placed on both sides of the target. The effect on the shielding experiment of interactions in these irradiation samples is negligible.

2.3 Particle, profile, structure and intensity of beam

A positively charged hadron beam consisting of a mixture of protons (34.8%), pions (60.7%) and kaons (4.5%) with momentum of 120 GeV/c impacted on the target. This beam is secondarily generated in a thin target by an accelerated proton beam, and only positive particles of the above momentum are transported to the CERF beam line. The beam profile was measured with a wire chamber, and has an approximately Gaussian distribution (σ_v = 9.16 mm, σ_h = 11.2 mm) with tails removed by a rectangular collimator. An alignment of the target was confirmed by putting a Polaroid film on the front surface of the copper target whenever the target location was changed.

Beam intensity can be changed by changing the width of the collimator located upstream of the beam transport line. This does not generate background neutrons for the CERF experiment. The cycle length is 16.8 seconds with a spill length of 4.8 seconds, and beam particles come uniformly in the spill.

2.4 PIC beam monitor

The number of incident beam particles was measured by a PIC (precision ionisation chamber) beam monitor. The beam intensity per PIC-count was calibrated to be about 2.3×10^4 beam particles. The uncertainty in the calibration factor is 0.4% [11]. The PIC monitor is located upstream of the target location B on the beam line.

3 Measurement of neutron energy spectra

3.1 Detector set-up

Neutron measurements were carried out using an NE213 organic liquid scintillator (12.7-cm diameter by 12.7-cm long) with an R4144 photomultiplier tube (Hamamatsu Photonics). Two NE102A plastic scintillators (veto counters) of rectangular shape and 5-mm thickness were used to reject charged particles from the beam line. A larger (30-cm by 30-cm) veto counter (L-Veto) was located upstream of the NE213 detector mainly to reject muon background, and a smaller (15-cm by 15-cm) veto counter (S-veto) was placed in front of the NE213 counter to reject charged particles (from the beam line) that penetrate the shielding wall or roof.

Figure 2 shows photos of the detectors set up for neutron energy spectra measurements behind the (a) iron shield roof and (b) concrete shield at 90 degrees from the copper target. The distances between the NE213 detector and shield surface were 3-cm and 7.5-cm for concrete and iron shield cases, respectively, as shown in Figure1. Figure 3 shows a sketch of the detectors set up behind the concrete shield with the interactions of neutron and charged particles.

3.2 Electronic measurement circuit

The electronic measurement circuit is shown in Figure 4. Two high voltage power supplies (ORTEC 556) were used for three PMTs (photomultipliers). One of them was used for the NE213 and S-veto counter, supplying -1 650 V. The other one supplied -1 500 V to the L-veto counter.

The anode signal from the NE213 detector was divided in two by a signal divider and fed to CFD1 (Constant fraction discriminator #1) and an ADC (Analogue to Digital Converter) through delay and attenuator modules. CFD1 rejected pulses lower than the threshold for the NE213 detector. Charged particle events (especially muons) from upstream, detected by the large veto counter (L-veto), were rejected in a coincidence module (Coin1). The next coincidence module (Coin2) rejected the events that occurred during the computer busy supplied by a GG (gate and delay generator). The signals to ADCs from the NE213 were total or slow components which were generated by gating in the total or the slow (decay) region of the signal pulse as shown in Figure 5. The signals from the small veto counter (S-veto) were fed to the ADC to get the total pulse height of charged particle events from the shield.

The ADC gate opens when the NE213-detector events do not coincide with the L-veto counter event or computer busy. The ADC accepts the NE213 pulses (total and slow component) and the S-veto pulses. The ADC data were recorded to the computer in event-by-event mode using the Kakuken On-line Data Acquisition System (KODAQ) [12].

The numbers of events from CFD1, Coin1 and Coin2 were counted by 3 scalers as shown in Figure 4. Scaler-1 counted the number of events of the NE213 detector whose pulses were above the threshold in CFD1. Scaler-2 counted the number of events after rejecting the L-veto events, and Scaler-3 counted the events remaining after rejecting the L-veto events and those occurring during computer busy. The number of events taken and recorded in the computer is equivalent to that on Scaler-3.

Muon events detected by the L-Veto counter were not recorded because they occurred too frequently and increased computer busy. Therefore, the L-veto events were only recorded during the initial stage of this experiment (in order to determine appropriate threshold for muon elimination). After setting the L-Veto threshold in CFD2, measurements were carried out with the INHIBIT-1 signal from CFD2 connected to Coin1 to reject the L-veto events automatically, as shown in Figure4.

3.3 Measurement location

One detector set was used for this experiment, and was located at different positions behind the shield (as shown in Figure 1) in order to measure neutron energy spectra behind different materials, thicknesses and angles from the target. The detector locations and their approximate angles with respect to the beam line (relative to the beam interaction points on the front surfaces of targets A and B) are given in Table 4. When the copper target was located at position B, measurements were carried out behind the 160-cm side concrete (B1-B3), 80-cm side concrete (B4, B5), and above the 40-cm iron roof (I1-I3). For target location A, measurements were carried out behind 80-cm thick concrete (A1-A3).

For the side concrete positions (A1-A3, B1-B5), the detector was located at the same height as the beam line, as shown in Figure 2(b). Above the iron roof (I1, I2, I3), the detector was located just above the beam line as shown in Figures 1 and 2(a). The detector location at I2′ above the 40-cm thick iron roof was off-axis at a transverse distance of 100-cm from the I2 location as shown in the upper part of Figure 1.

3.4 Neutron background measurement

Charged-particle and photon events detected by the NE213 detector can be rejected in offline analysis as described in Sections 4.1 and 4.2. However, neutrons originating from beam losses in neighbouring beam lines, which might be included in the measured data, also need to be eliminated. The neutron background measurements at each detector position were carried out with no beam in H6 (our beam line), thus only accounting for contributions from neighbouring beam lines (H4 and H8). For normalisation purposes, the number of beam spills was counted both for normal and background measurements. The beam intensities at the targets in the neighbouring beam lines (H4 and H8) were observed to confirm the background stability during both the normal and background measurements.

4 Data analysis

Event-by-event data recorded in the measurement contains the following three values in each event:

- NE213 total pulse height (Total);
- NE213 slow component (Slow);
- S-veto total pulse height (S-veto).

These data were sorted to one or two-dimensional distributions for various types of analysis.

4.1 Charged particle discrimination

Event-by-event data were sorted to two-dimensional distributions (2-D plots) of S-veto or L-veto versus Total, and one-dimensional distributions for the two veto counters as shown in Figure 6.

Figure 6(a) shows events, recorded during the initial stage of the experiment for tune up the circuit, in which there is a coincidence between the L-veto counter and the NE213 detector. The muon component can be seen above roughly channel 180, and these events should be rejected. Using this information, the threshold of CFD2 in Figure 4 was determined during the experiment, and used to make the INHIBIT-1 signals for CFD1.

In Figure 6(b), events due to charged particles that penetrated the shielding can be seen above roughly channel 150 in the S-veto pulse height distribution. These charged-particle events were recorded in all the measurements, and they were rejected in the analysis.

4.2 N-γ separation

Figure 7 shows a 2-D plot of the Total versus Slow components of the NE213 signals along with a magnified view of the low channel region. Since the slow component was obtained by integrating the decay part of the detector signal pulse as shown in Figure 5, electron events generated from γ-rays appear in lower channels and are clearly separated from protons, deuterons and alpha events generated by neutrons. Background muons coming from directions which were not covered by the two veto counters also contribute to the electron component and can be rejected in this process.

The neutron events were selected by eliminating the electron and muon events from the 2-D plot in Figure 7. In this process, escaping-protons (which go out through the detector wall) are also eliminated because the pulse shape of the signal of the escaping-protons is close to that of electrons and therefore the escaping-proton events overlap in the electron events [13], as shown in Figure 7. This does not affect final results because the escaping-proton component is not included in the response functions [14] used in this unfolding analysis, either.

4.3 Light output calibration

A light output calibration is generally performed to convert the ADC channel into a light unit in MeVee (MeV electron equivalent) using the reference light outputs. The ^{60}Co light output corresponding to 1.15 MeVee is determined to be the channel having 0.303 times the counts of the Compton edge due to 1.17 and 1.33 MeV γ-ray from ^{60}Co. The ^{241}Am-Be light output corresponding to 4.2 MeVee is determined to be the channel having 0.664 times the counts of the Compton edge due to 4.43 MeV γ-ray from ^{241}Am-Be. A 0-point (0 MeVee), which is independent of the supplied high voltage or gain, can be measured by putting a 50Ω terminator on the ADC. More details about calibration are described in Ref. [15].

4.4 Normalisation

Three scalers were placed in the measurement circuit as shown in Figure 4. The total number of events detected by the NE213 scintillator for each run was recorded by Scaler-1. The number of event triggers was recorded by Scaler-2, and does not include those events that are coincident with the L-Veto counter (mostly muon event). The number of events recorded in the computer was measured by Scaler-3. Not included are events that occurred during computer busy. Computer live ratio, that is the ratio of the number of recorded events to the number of triggered events, is used to correct for counting loss due to computer-busy. The number of incident beam particles was obtained using the calibration factor of 2.3×10^4 beam particles per PIC beam monitor count. After scaling by the "Computer live ratio", the corrected number of incident beam particles for the corresponding recorded event data was obtained.

In the background runs, PIC beam monitor counts were not available (there was no beam on the target). In order to get normalisation factors for background runs, the "expected" number of the incident beam particles for the background run was estimated using a ratio of the number of beam particle to the number of spills during the normal and background measurements. This worked properly since stabilities could be confirmed for the beam intensities at the targets in the neighbouring beam lines (H4 and H8) from SPS log data during both for normal and background measurements in each location. The neutron-background subtraction process will be described in Section 4.7.

More details about normalisation process with numerical data tables for each run are described in Ref. [15].

4.5 Probability of pulse pile-up

This section describes the possibility of pulse pile-up in the NE213 scintillator during the measurements, which decreases detector efficiency. The following two possibilities are discussed here to clarify the pile-up issues:

- chance coincidence from high intensity, especially due to of muon background;
- coincidence due to multiple secondary-particle productions by the high energy beam.

More details about pulse pile up analysis process with numerical data tables for each run are described in Ref. [15].

4.5.1 Coincidence from high beam intensity

From the trigger ratio (the ratio of the number of triggers to the total number of NE213 detector events), the fraction of muon events can be roughly estimated since the events that coincide with the L-Veto counter were vetoed in the trigger circuit. For example, 62% of detected events were rejected in the

circuit in I3 measurement, as reflected in the trigger ratio of 0.38. This run had the highest count rate (11 764 count/sec). The count rates are already corrected with the beam spill period of 4.8 seconds during the 16.8 sec cycle as described in Section 2.3. Muons come from upstream uniformly during the beam spill.

From Ref. [16], the probability of escaping from pile-up P(0) is expressed as follows when the interactions occur uniformly in time:

$$P(0) = \exp(- n \tau) \quad (1)$$

where n is the interaction rate in the detector and τ is the resolution time (100 nsec).

The resolution time is ~100 nsec, which is the ADC gate width for the total pulse-height of the NE213 as shown in Figure 5. Using Equation (1), the count rate is described as:

$$m = n \exp(- n \tau) \quad (2)$$

where m is the count rate in the detector (11 764 count).

When m = 11 764, n = 11 778 is given from Equation (2). Therefore, P(0) = 0.9988 from Equation (1). That means the pile up probability is 0.12%. We conclude that this chance coincidence is negligible.

4.5.2 Multiple secondary-particle production

Even one interaction of a high energy beam particle on the target produces hundreds of secondary particles from the target simultaneously. This multiplicity is independent of the beam intensity. The pile-up possibility is very high inside the tunnel, especially in the forward direction. Here, the pile-up possibility outside the shield in the lateral direction is verified for the case of this experiment.

There are two possible cases that reduce detection efficiency due to pile-up:

1) If a neutron is detected with a proton simultaneously as shown in the sketch of Figure 3, one piled-up pulse is recorded, but this event would be rejected in the analysis due to the proton's interaction with the S-veto counter.

   Interaction: 1 neutron, 1 proton → recoded event: 1 → analysed event: 0

2) If two neutrons are detected, one piled-up pulse is recorded.

   Interaction: 2 neutrons → recoded event: 1 → analysed event: 1

Both (1) and (2) can be clarified using 2-D plots of the total vs. the slow component of the NE213 detector, as shown in Figure 8. This distribution shows all the recorded event data, including charged particles which would be eliminated later by the S-veto threshold (see Section 4.1).

In this experiment, pulse pile up occurs if more than two pulses come during the gate opening as shown in Figure 9, even if pulses are not piled up physically such as (b) in Figure 9. In this case, although both total and slow components increase their integrations, the slow component increases a lot more because the peak part of the following pulse is also involved. As shown in Figure 8, therefore, pile-up events appear in the higher channel region of the slow-component in the 2-D plot [8]. Figure 10 shows a total pulse-height distribution of pile-up events for the location B5 (Run26), which is the most forward (smallest angle) position from the target, compared with raw data. It can be seen that the pile-up event component is negligible, and all other measurements have less amount of the component than that of location B5.

4.6 Response function matrix

The numerical data of the response matrix which was made from the response functions of the NE213 scintillator which have been measured in the neutron energy range up to 390 MeV at the RCNP cyclotron facility at Osaka University [14]. The matrix contains 19 light output groups for 18 neutron energy groups from 12 to 380 MeV. The uncertainty of the response function is 15%.

However, in the shielding experiment, since some of neutrons come from the side direction especially for location B4 and B5, detector response in the shielding experiment might be slightly different from the measured response functions by parallel neutron beam from front surface.

4.7 Neutron background subtraction

The normalisations for normal and background measurements were already described in Section 4.4. The light-output distributions bunched in light energy group of the response matrix after background subtractions were used in the unfolding. Actually, the background subtractions and group bunching process mentioned above were carried out at the same time during the unfolding process described in the next section. Figures of the light-output distributions for normal and background of each run are described in Ref. [15].

The neutron background originated from the beam line adjacent to ours (outside our beam line's shielding), and it depended on the neighbouring beam intensity and on our detector location. More background contribution at location A (where the concrete side shielding is thinner) and at location I above the roof than was observed at locations B1-B3. Although no background measurements were performed at B1 and B3, the background at these locations, like that at B2, is considered to be negligible due to the thick shielding.

4.8 Unfolding

Neutron energy spectra were obtained by the unfolding method using the FORIST code [17]. A window function makes the unfolded neutron spectra smoother without the fluctuations which are caused by uncertainties in the light calibration, response function and the measured pulse-height distribution. In this work, in order to avoid fluctuation, and also in order not to lose the original spectral shape, a 30% window was given for most of the neutron energy groups.

4.9 Uncertainty

The statistics of the measured light output distribution (normal and background) and the uncertainty due to the unfolding process are already taken into account in the errors of the flux of each energy bin of the neutron energy spectra obtained by the FORIST code. In addition, an error in the absolute value of the response function (15%) was added in vector for all fluxes in each energy bin.

Neutron attenuation due to any interactions in the veto counter was assumed to be negligible in the analysis, but further investigation by simulation should be needed to prove it.

5 Results and discussions

The measured neutron energy spectra obtained by the unfolding method are shown in Figure 11 for 40-cm thick iron, 80- and 160-cm thick concrete. Although the unfolded neutron spectra were obtained from 12-380 MeV, the spectra below 30 MeV have a large uncertainty since the maximum light outputs of the response functions below 30 MeV are too close to their threshold. Therefore, only the unfolded neutron energy spectra above 32 MeV were employed as final results. Also, since the maximum neutron energy of the response matrix is 380 MeV, the experimental data above this energy could not be obtained. Bumps in the fluxes around the maximum energy can be seen in the spectra at forward angles below 50 degrees since neutrons with energy higher than 380 MeV are not negligible and contribute to the results of the maximum energy group in the unfolding process. For the results in the other lateral locations, neutron fluxes above 380 MeV are negligible, and no significant bump can be seen. Improved neutron spectra are expected to be obtained when extended response functions with wider neutron energy range are available in the future.

In terms of the absolute neutron flux, further investigation of detector response simulation is needed, especially above 100-MeV neutron energy, since the resulted neutron flux strongly depends on the measured response functions which were normalised by simulation results. Moreover, detector response might slightly change due to side injection and it should be also investigated in the future experiment and simulation.

6 Summary

High energy neutron measurements were performed at various locations behind lateral shields of concrete and iron using a 120 GeV/c hadron beam at the CERF facility at CERN, and energy spectra in the energy range from 32 to 380 MeV were obtained by an unfolding method.

The CERF facility has a simple structure of beam line and shielding, and the source term is clearly defined. This experiment explored different angles, shielding materials and thicknesses. The radiation field at CERF has been measured over many years with different instruments and this experiment provides a valuable extension towards spectral measurements of high energy neutrons.

The used spectrometer, the NE213, is an instrument which has been widely used for numerous measurements, it is well-tested and understood. However, in such a high energy beam facility, there were many difficulties of the measurements such as significant muon background and the pile-up of events within the same particles shower, and also difficulties of unfolding analysis with measured response functions which is hardly available above 20 MeV.

This experiment provides valuable data in order to benchmark Monte Carlo transport codes and evaluate their accuracy in this aspect. A first benchmark study is discussed in Ref [18].

Acknowledgements

This work was supported by Department of Energy contract DE-AC02-76SF00515. We would like to thank the members of the Radiation Protection group at CERN for their great help in this experiment.

References

[1] N. Nakao, H. Nakashima, T. Nakamura, Sh. Tanaka, Su. Tanaka, K. Shin, M. Baba, Y. Sakamoto, Y. Nakane, "Transmission Through Shields of Quasi-monoenergetic Neutrons Generated by 43- and 68-MeV Protons: Part I – Concrete Shielding Experiment and Calculation for Practical Application", *Nucl. Sci. Eng.*, 124 (1996) pp. 228-242.

[2] H. Nakashima, N. Nakao, Sh. Tanaka, T. Nakamura, K. Shin, Su. Tanaka, H. Takada, S. Meigo, Y. Sakamoto, Y. Nakane, M. Baba, "Transmission Through Shields of Quasi-monoenergetic Neutrons Generated by 43- and 68-MeV Protons: Part II – Iron Shielding Experiment and Analysis for Investigating Calculation Methods and Cross Section Data", *Nucl. Sci. Eng.*, 124 (1996), pp. 243-257.

[3] N. Nakao, M. Nakao, H. Nakashima, Su. Tanaka, Y. Sakamoto, Y. Nakane, Sh. Tanaka, T. Nakamura, "Measurements and Calculations of Neutron Energy Spectra Behind Polyethylene Shields Bombarded by 40- and 65-MeV Quasi-monoenergetic Neutron Sources", *J. Nucl. Sci. Technol.*, 34 (4) (1997) pp. 348-359.

[4] T. Nunomiya, N. Nakao, P. Wright, T. Nakamura, E. Kim, T. Kurosawa, S. Taniguchi, M. Sasaki, H. Iwase, Y. Uwamino, T. Shibata, S. Ito, D.R. Perry, "Measurement of Deep Penetration of Neutrons Produced by 800-MeV Proton Beam Through Concrete and Iron at ISIS", *Nucl. Instr. Meth.*, B 179 (2001) pp. 89-102.

[5] T. Nunomiya, N. Nakao, P. Wright, T. Nakamura, E. Kim, T. Kurosawa, S. Taniguchi, M. Sasaki, H. Iwase, T. Shibata, Y. Uwamino, S. Ito, D.R. Perry, *Experimental Data of Deep-penetration Neutrons Through Concrete and Iron Shield at ISIS Spallation Neutron Source Facility Using an 800-MeV Proton Beam*, KEK Report 2001-24 (Feb. 2002).

[6] M. Sasaki, N. Nakao, T. Nunomiya, T. Nakamura, A. Fukumura, M. Takada, "Measurements of High-energy Neutrons Penetrated Through Iron Shields Using Self-TOF Detector and an NE213 Organic Liquid Scintillator", *Nucl. Instr. Meth.*, B 196 (2002) pp. 113-124.

[7] H. Nakashima, *et al.*, "Current Status of the AGS Spallation Target Experiment", *Proc. of OECD/NEA Workshop on Shielding Aspects on Accelerator, Targets and Irradiation Facilities (SATIF-6)*, SLAC, Stanford, CA, USA, 10-12 April 2002, pp. 27-36, OECD/NEA, Paris (2003).

[8] S. Taniguchi, T. Nakamura, T. Nunomiya, H. Iwase, S. Yonai, M. Sasaki, S.H. Rokni, J.C. Liu, K.R. Kase, S. Roesler, "Neutron Energy and Time-of-flight Spectra Behind the Lateral Shield of a High Energy Electron Accelerator Beam Dump", *Nucl. Instr. Meth.*, A 503 (2003) pp. 595-605.

[9] N. Nakao, *et al.*, "Arrangement of High-energy Neutron Irradiation Field and Shielding Experiment Using 4 m Concrete at KENS", *Proc. 10th International Conference on Radation Shielding (ICRS10)*, Madeira, Portugal, 9-14 May 2004; *Radiat. Prot. Dosim.,* Vol. 116, No. 1-4, pp. 553-557 (2005).

[10] A. Mitaroff, M. Silari, "The CERN-EU High Energy Reference Field (CERF) Facility for Dosimetry at Commercial Flight Altitudes and in Space", *Radiat. Prot. Dosim.*, 102, No. 1, 7-22 (2002).

[11] Helmut Vincke, *et al.*, *Accurate PIC Calibration by the Use of a Coincidence of Two Scintillators*, CERN-SC-2004-090-RP-TN, CERN (2004).

[12] K. Omata, *et al.*, *A Data Acquisition System Based on Personal Computer*, INS-REP-884, Institute for Nuclear Study, University of Tokyo (1991).

[13] N. Nakao, T. Kurosawa, T. Nakamura, Y. Uwamino, "Absolute Measurements of the Response Function of an NE213 Organic Liquid Scintillator for the Neutron Energy Range up to 206 MeV", *Nucl. Instr. and Meth.*, A 463 (2001) pp. 275-278.

[14] S. Taniguchi, N. Nakao, H. Yamakawa, K. Oishi, T. Nakamura, A. Tamii, K. Hatanaka, T. Saito, "Measurement of Response Functions of Organic Liquid Scintillator for Neutron Energy Range up to 390 MeV", *Proceedings of AccApp05*, Venice, Italy, 29 August-1 September 2005.

[15] N. Nakao, S. Taniguchi, S.H. Rokni, S. Roesler, M. Brugger, M. Hagiwara, H. Vincke, H. Khater, A.A. Prinz, "Measurement of Neutron Energy Spectra Behind Shielding at 120 GeV/c Hadron Beam Facility, CERF", Slac *Radiation Physics Note*, RP-06-06 (2006).

[16] Glenn F. Knoll, *Radiation Detection and Measurement, 3rd edition*, John Wiley and Sons Inc. (2000).

[17] R.H. Johnson, *FORIST, Neutron Spectrum Unfolding Code (FERDOR with Optimized Resolution Using an Iterative Smoothing Technique)*, PSR-92, RSIC/ORNL (1976).

[18] N. Nakao, S.H. Rokni, M. Brugger, S. Roesler, H. Vincke, K. Kosako, "Calculation of High-energy Neutron Spectra with Different Monte Carlo Transport Codes and Comparison to Experimental Data Obtained at the CERF Facility", these proceedings.

Table 1: Recent shielding experiments at high energy accelerator facilities

Facility **Institution** **Country** **Year of experiment** **Reference**		TIARA JAERI Japan 1992-1996 [1,2.3]	ISIS RAL UK 1998 [4,5]	HIMAC NIRS Japan 1998-2000 [6]	AGS BNL USA 2001 [7]	FFTB SLAC USA 2001-2002 [8]	KENS KEK Japan 2003 [9]	CERF CERN Switzerland 2004 This work
Accelerator		Proton Cyclotron	Synchrotron (spallation source)	Heavy ion Synchrotron	Alternating Gradient synchrotron	Electron Linac	Synchrotron (spallation source)	Super Proton Synchrotron (SPS)
Particle		p^+	p^+	$^{12}C^{6+}$	p^+	e^-	p^+	p^+, π^+
Energy		45, 68 MeV	800 MeV	400 MeV/n	2.83, 24 GeV	28.7 GeV	500 MeV	120 GeV/c
Target	**Thin** **Thick**	^{7}Li	Ta	Graphite	Ag	Al	W	Cu
Beam angle to the shield		0°	90°	0°	90°	90°	0°	13-133°
Shield (cm)	**Concrete**	25-200	20-120	50-250	50-500	274-396	40-400	80, 160
	Iron	10-130	10-60	10-130	25-330			40
	Polyethylene	30-183						
Detector	**NE213**	5"ϕ x 5"		5"ϕ x 5"		5"ϕ x 5"		5"ϕ x 5"
	Bonner sphere	He-3 counter	Indium activation			^{6}Li glass counter		
	Self-TOF			Self-TOF				
	Activation foil		Bi, C, Al	Bi	Bi, Co, Au Al, In		Bi, Al, In, Au	
Energy spectra (MeV)	**NE213**	5-68		20-800		6-800		32-380
	Bonner sphere	(thermal)-70	(thermal)-400			(thermal)-400		
	Self-TOF			100-600				
	Bi-activation			20-1000				
Activation reaction rate			Yes		Yes		Yes	

JAERI: Japan Atomic Energy Research Institute, Japan, RAL: Rutherford Appleton Laboratory, UK, NIRS: National Institute of Radiological Sciences, Japan, BNL: Brookhaven National Laboratory, USA, SLAC: Stanford Linear Accelerator Center, USA, KEK: Kou Enerugi Kasokuki Kenkyu Kikou (High Energy Accelerator Research Organisation), Japan, CERN: European Organisation for Nuclear Research, Switzerland.

Table 2: Densities of materials

Material	**Density [g/cm^3]**
Copper target	8.96
Iron roof (upper)	7.65
Iron roof (lower)	7.20
Concrete shield (see Table 2)	2.40

Table 3: Typical composition of the concrete shielding at CERN (2.40 g/cm^3)

	[wt.%]	**[atom/cm^3]**		**[wt.%]**	**[atom/cm^3]**
H	0.561	8.04E+23	Si	16.175	8.32E+23
C	4.377	5.27E+23	S	0.414	1.87E+22
O	48.204	4.35E+24	K	0.833	3.08E+22
Na	0.446	2.80E+22	Ca	23.929	8.63E+23
Mg	1.512	8.99E+22	Ti	0.173	5.22E+21
Al	2.113	1.13E+23	Fe	1.263	3.27E+22

Table 4: Detector locations and angles with respect to the beam line and target front surface in the respective target positions

		Side concrete						Iron roof			
		80-cm thick			160-cm thick			40-cm thick			
Target A	Location	A3	A2	A1							
	Angle	40°	90°	133°							
Target B	Location	B5		B4	B3	B2	B1	I3	I2	I2'	I1
	Angle	13°		26°	50°	90°	110°	35°	90°	90°	130°

Figure 1: Geometry of the CERF facility and detector locations. Beam comes from Q to P in the beam line in the figure.

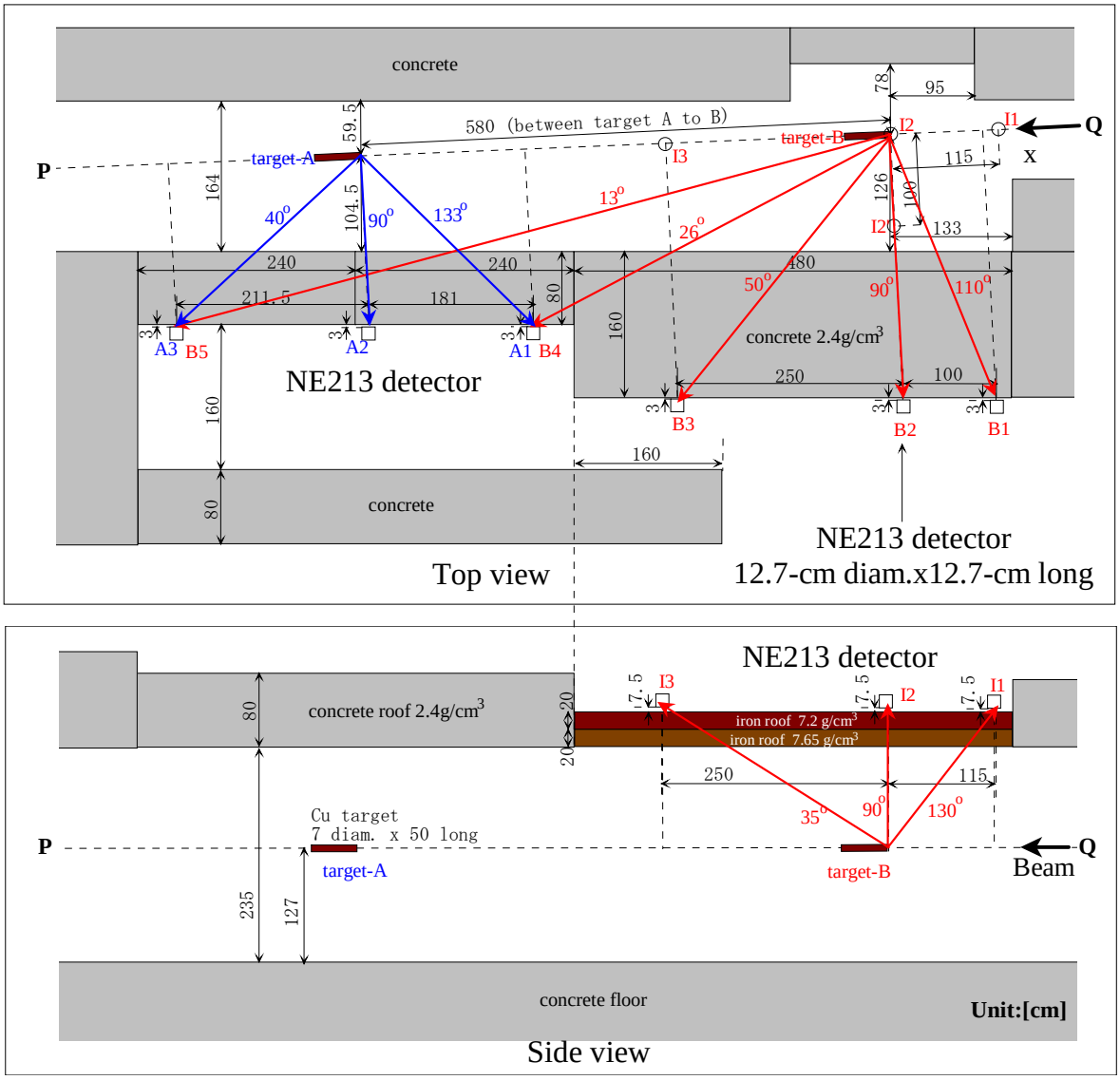

Figure 2: Detectors set up (a) above the iron roof and (b) at the side concrete

The stainless steel plate below the NE213 detector in figure (a) has a hole (15-cm diameter) in the centre, and no neutron attenuation occurs

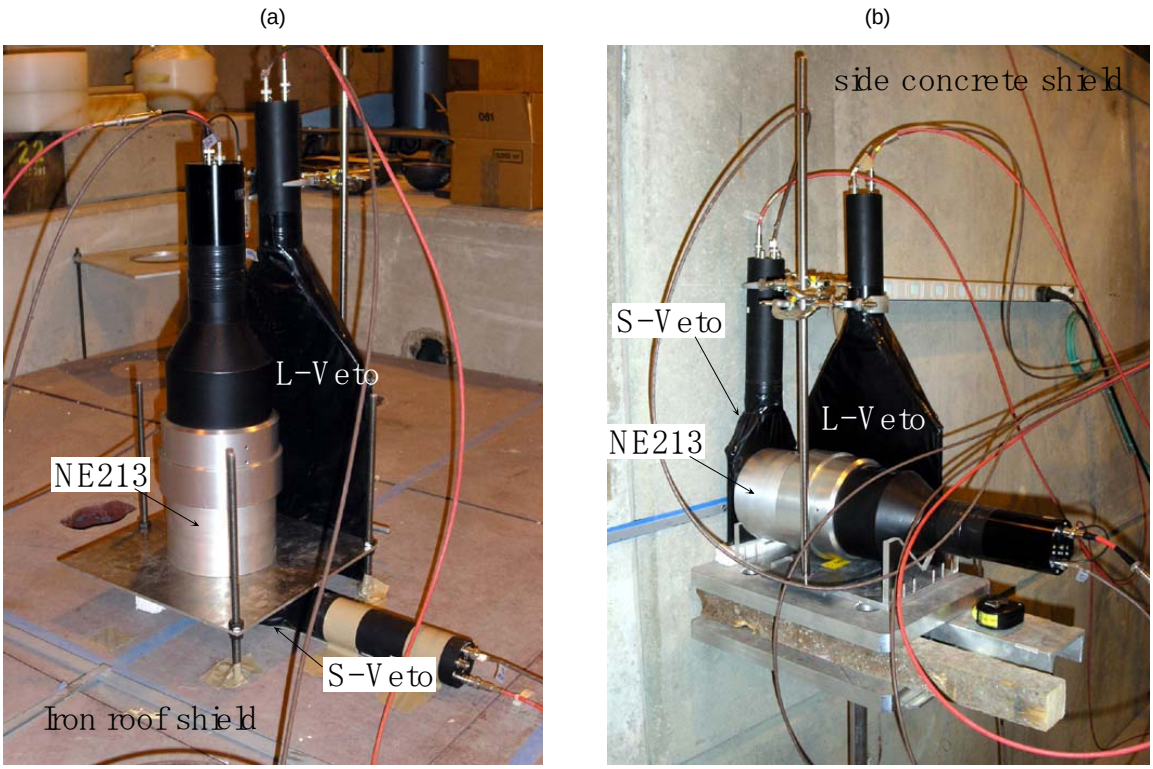

Figure 3: Sketch of the detectors set-up with the interactions of neutron and charged particles

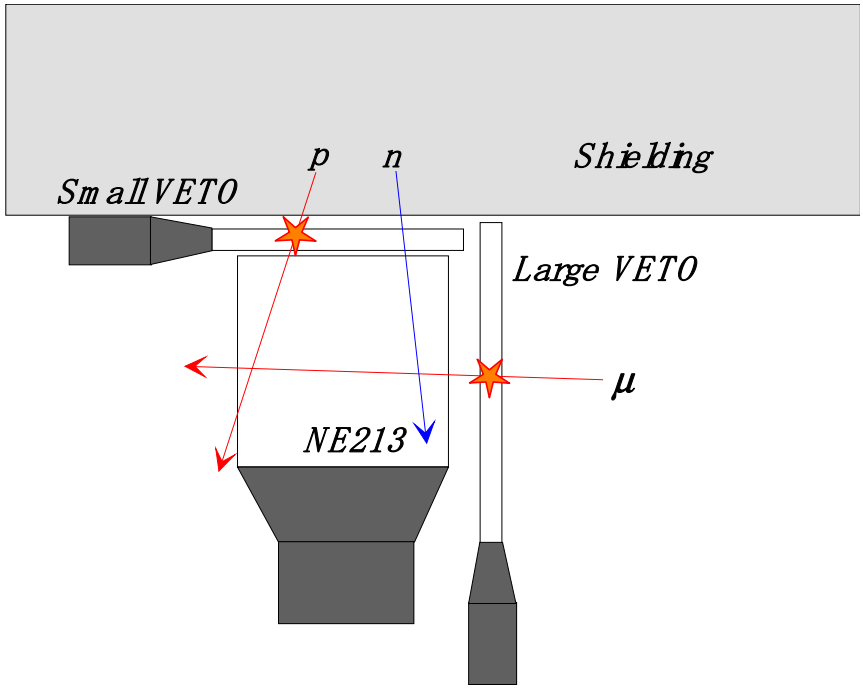

Figure 4: Electronic measurement circuit

PMT: photo multiplier, HV: High voltage power supply, CFD: constant fraction discriminator (ORTEC935), COIN: coincidence, GG: gate and delay generator, DIV: signal divider, INV: inverter, DLY: delay, ATT: attenuator, ADC: analogue to digital converter (LeCroy2249W). In the beginning of the experiment, L-veto event was recorded with ADC connection without INHIBIT-1 connection.

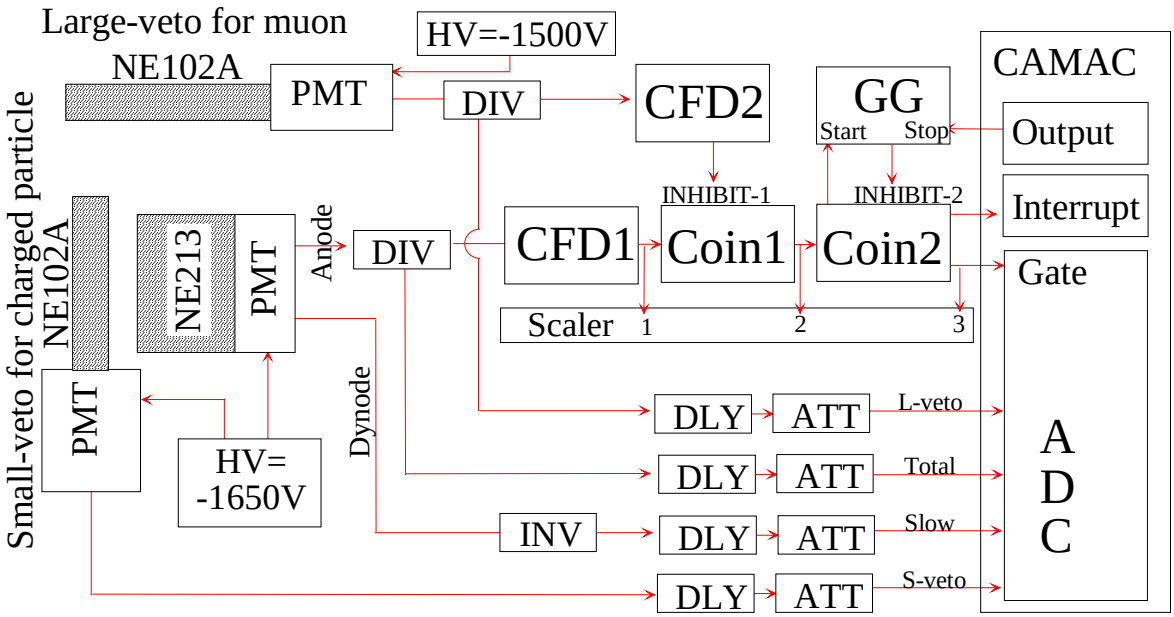

Figure 5: The signals from the NE213 to ADC which were gated in the total pulse height and the slow (decay) component regions

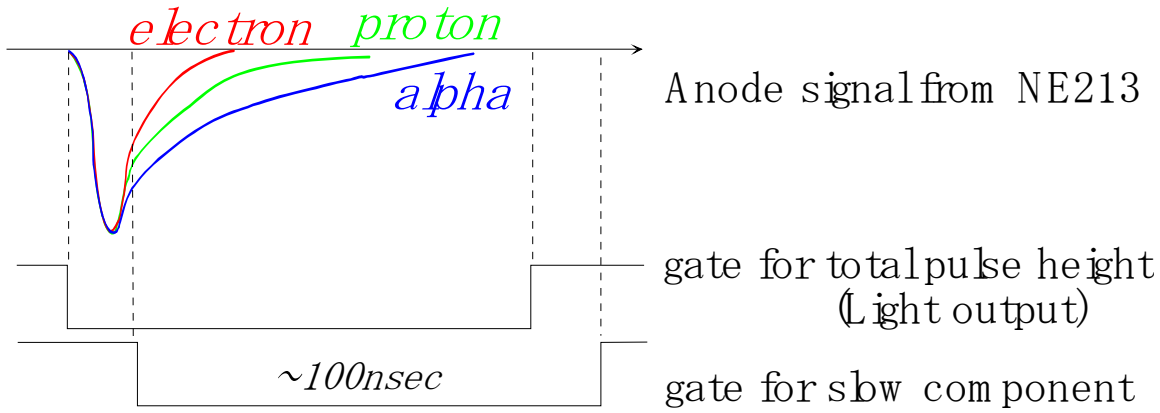

Figure 6: Two-dimensional distributions of veto-counters versus NE213 total pulse height (light output) and one-dimensional distributions of veto-counters for (a) L-veto and (b) S-veto

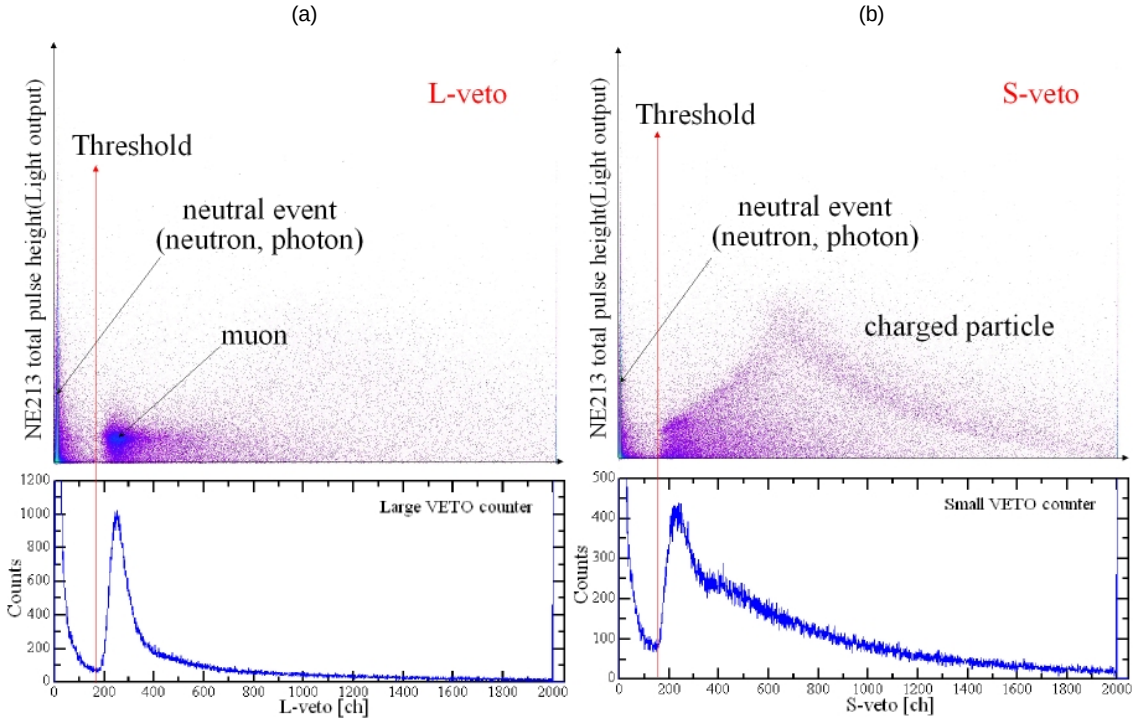

Figure 7: Two dimensional distributions of slow component versus total pulse height of NE213 detector signal for (a) whole region and (b) magnified low channel region

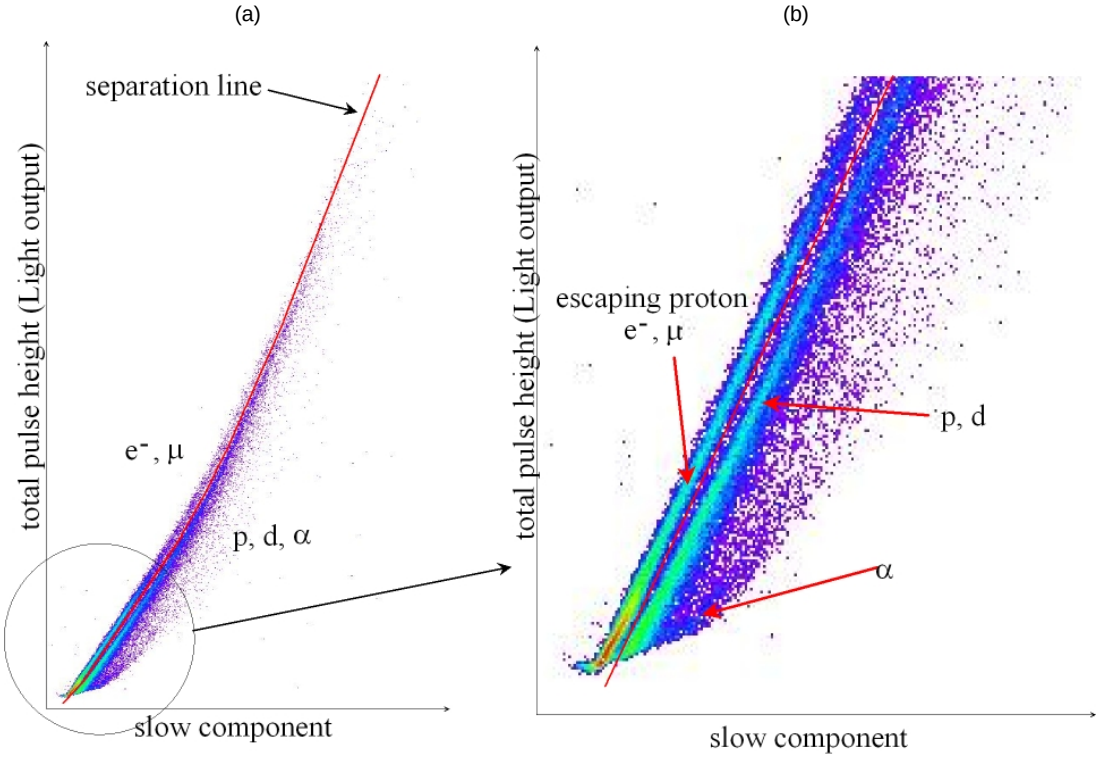

Figure 8: Pile-up event selection from the two-dimensional distributions of slow component versus total pulse height of NE213 detector signal

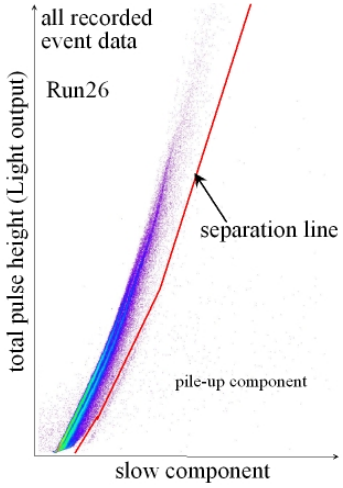

Figure 9: Sketch of pile-up pulses during the ADC gates

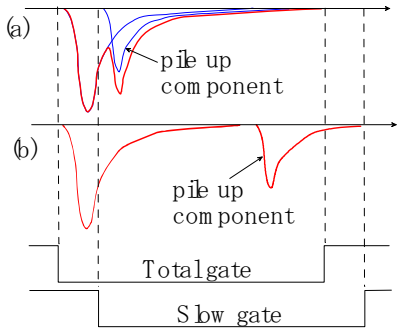

Figure 10: Total pulse-height distributions for the raw data and pile-up events selected from two-dimensional distribution shown in Figure 8

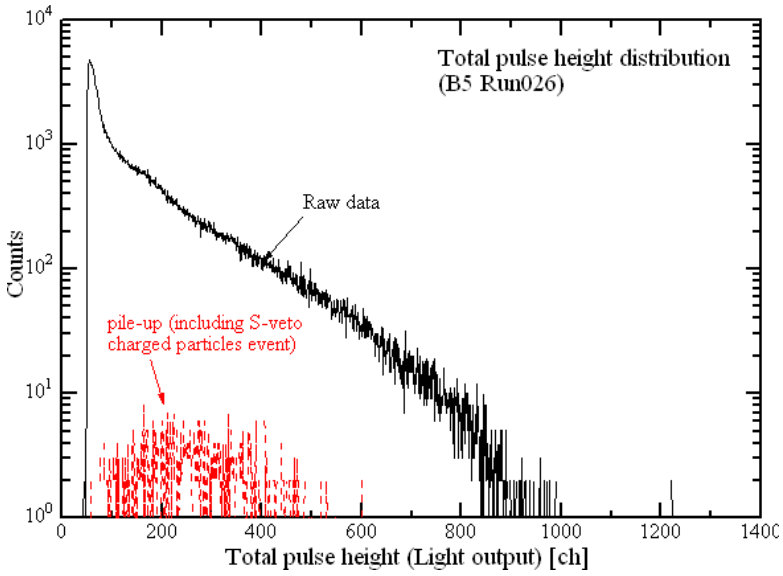

Figure 11: Experimental neutron energy spectra behind (a) 40-cm thick iron, (b) 80-cm thick concrete and (c) 160-cm thick concrete